Pattern Recognition 51 (2016) 27–42

Contents lists available at ScienceDirect

Pattern Recognition

journal homepage: www.elsevier.com/locate/pr

A variational model with hybrid images data fitting energies for segmentation of images with intensity inhomogeneity

Haider Ali [a], Noor Badshah [b,*], Ke Chen [c], Gulzar Ali Khan [a]

[a] Department of Mathematics, University of Peshawar, Pakistan
[b] Department of Basic Sciences, UET Peshawar, Pakistan
[c] Centre for Mathematical Imaging Techniques and Department of Mathematical Sciences, The University of Liverpool, United Kingdom

ARTICLE INFO

Article history:
Received 1 May 2014
Received in revised form
10 July 2015
Accepted 19 August 2015
Available online 5 September 2015

Keywords:
Image segmentation
Calculus of variations
Level set method
Partial differential equations
Edges
Objects

ABSTRACT

Level set functions based variational image segmentation models provide reliable methods to capture boundaries of objects/regions in a given image, provided that the underlying intensity has homogeneity. The case of images with essentially piecewise constant intensities is satisfactorily dealt with in the well-known work of Chan–Vese (2001) and its many variants. However for images with intensity inhomogeneity or multiphases within the foreground of objects, such models become inadequate because the detected edges and even phases do not represent objects and are hence not meaningful. To deal with such problems, in this paper, we have proposed a new variational model with two fitting terms based on regions and edges enhanced quantities respectively from multiplicative and difference images. Tests and comparisons will show that our new model outperforms two previous models. Both synthetic and real life images are used to illustrate the reliability and advantages of our new model.

1. Introduction

Image segmentation is the task of dividing an image into different regions such that each region is homogeneous in color, intensity or texture. The aim is to select specific features out of an image from distinguishing them from the background [1–7]. Various models have been developed for image segmentation tasks. The Mumford–Shah functional minimization [5], the snake model [8], region growing and emerging [9], watershed algorithms [10], minimum description length criteria [6], graph cuts [11] and Markov Random Fields [12] are some examples [13]. Edge detection based on an edge detector function of the gradient of a given image provides effective segmentation methods in some cases but often such a function is used in many other models [3,14,15].

Our main concern here is on region based segmentation models in which objects are detected by optimizing regional homogeneity using some special terms. Such terms are named as region detectors or fidelity terms. There is a rich literature on fidelity terms with the statistical variance as a common choice. The most influential and the best known among the segmentation models is the Mumford–Shah (MS) model [5]. Minimization of the MS functional leads to a new segmentation image which is very close to the original image with boundaries of minimal length and objects having minimal variation. It should be remarked that there exist many approaches to combine the advantages of both edge-based and region-based models [3,16,17].

In MS formulation, for a given image u_0, we construct an image $u : \Omega \to \mathbb{R}$ and a set of edges $K \subset \Omega$ by minimizing

$$F(u,K)^{MS} = \int_{\Omega} (u-u_0)^2 \, dx\, dy + \alpha \int_{\Omega\setminus K} |\nabla u|^2 \, dx\, dy + \beta \int_K ds \qquad (1)$$

where α and β are positive. Here the first term is the fidelity term which keeps the solution image u as close as possible to the given image u_0, the second term is the regularizer which helps to give the solution image u smooth in the region $\Omega\setminus K$ inside the objects away from edges and the third is the length term, which helps to filter out false edges and to ensure solution uniqueness. With this mechanism, whenever an image u_0 is segmented, a piecewise smooth image u is obtained with edge information in K. In other words, a cartoon version u of the given image u_0 is obtained. Up to now, the MS model has not been solved directly (i.e. without approximations).

* Corresponding author.
E-mail addresses: haider_uop99@yahoo.com (H. Ali), noor2knoor@gmail.com (N. Badshah), mshahkar95@yahoo.com (G.A. Khan).
URL: http://www.liv.ac.uk/cmit (K. Chen).

http://dx.doi.org/10.1016/j.patcog.2015.08.022
0031-3203/

The Chan–Vese model (CV) model [2] (which can be solved directly) is a special case of the MS model [5] by representing the set K as the boundary Γ which separates Ω of a given image $u_0(x,y)$ into two subdomains $inside(\Gamma)$ and $outside(\Gamma)$. The CV model minimizes

$$F^{CV}(c_1,c_2,\Gamma)=\lambda_1\int_{inside(\Gamma)}|u_0-c_1|^2\,dx + \lambda_2\int_{outside(\Gamma)}|u_0-c_2|^2\,dx+\mu\ \text{length}(\Gamma) \quad (2)$$

where c_1 and c_2 are the average intensities in $inside(\Gamma)$ and $outside(\Gamma)$ respectively, $\mu\geq 0,\lambda_1>0,\lambda_2>0$ are fixed parameters, μ controls the size of objects and λ_1,λ_2 control the image data driven force inside and outside the contour respectively.

Let $\phi(x,y)$ be a level set function [18,19] such that $\Gamma=\{(x,y)\in\Omega:\phi(x,y)=0\}$ and

$$inside(\Gamma)=\{(x,y)\in\Omega:\phi(x,y)>0\},$$
$$outside(\Gamma)=\{(x,y)\in\Omega:\phi(x,y)<0\}. \quad (3)$$

Using ϕ can simplify Eq. (2). By minimizing $F^{CV}(c_1,c_2,\phi)$, we obtain c_1 and c_2

$$c_1=\frac{\int_\Omega u_0H(\phi)\,dx\,dy}{\int_\Omega H(\phi)\,dx\,dy},\quad c_2=\frac{\int_\Omega u_0(1-H(\phi))\,dx\,dy}{\int_\Omega(1-H(\phi))\,dx\,dy}.$$

Then minimization with respect to ϕ leads to the following equation:

$$\delta(\phi)\left[\mu\nabla\cdot\left(\frac{\nabla\phi}{|\nabla\phi|}\right)-\lambda_1(u_0-c_1)^2+\lambda_2(u_0-c_2)^2\right]=0. \quad (4)$$

Formally $H(\phi)$ is the Heaviside function and $\delta(\phi)$ is the dirac delta function. For differentiability, regularized Heaviside and delta are used as given by

$$H_\epsilon(z)=\frac{1}{2}\left(1+\frac{2}{\pi}\arctan\left(\frac{z}{\epsilon}\right)\right),\quad \delta_\epsilon(z)=\frac{\epsilon}{\pi(\epsilon^2+z^2)}. \quad (5)$$

Although the CV model is non-convex, it has been widely used and has successfully solved many practical problems as long as the image intensities are close to piecewise constant.

However, beyond its original assumption, extending the CV model to segment images having objects with inhomogeneous intensities has been the subject of several recent works [1,3,20]. To motivate this paper, in Fig. 1, we show two images which cannot be segmented satisfactorily by the CV model. One may argue that segmentations are successful in the sense that the correct boundaries for the dark regions are identified but we desire to segment the objects (not just dark edges, which do not locate the complete object); in this sense, even a multiphase model for piecewise constant intensities would give incorrect results due to getting redundant edges inside an object. We shall propose a new model that extends the TV work.

The rest of this paper is organized in the following way. Section 2 briefly reviews three recent works that attempted to extend the TV model. Section 3 presents our proposed model, though based on the CV, that is capable of segmentation images with low contrast, inhomogeneous intensities, or noise and edges in multiple phases. We give some details of numerical solution by an additive operator spitting method. Section 4 reveals the fast global minimization frame work implementation for the proposed model. Section 5 gives some final test results for comparing our proposed model with other related models, showing the reliability and robustness of the new model for a range of challenging images. For quantitative comparison of segmentation results, section 6 discusses the Jaccard similarity. Finally the conclusion is made in Section 7.

2. Some recent works for extension of the TV model

Extension of the TV model may be done in a number of ways. Here we review two ideas which use different fidelity terms since the previous terms $(u_0-c_j)^2$ alone are not adequate.

2.1. The coefficient of variation (COV) based model

For image u_0, its coefficient of variation (based on the variance and the mean) defined by

$$\frac{var(u_0)}{mean(u_0)}$$

is relatively large in regions which contain the object edges and small in other regions where there are no strong edges (gradients). These relative quantities do not reply on the assumption that u_0 has piecewise constant intensities. Making use of this observation, in [1], we proposed the new fidelity terms

$$\int_{inside(\Gamma)}\frac{(u_0(x,y)-c_1)^2}{c_1^2}\,dx\,dy+\int_{out(\Gamma)}\frac{(u_0(x,y)-c_2)^2}{c_2^2}\,dx\,dy$$

and consequently a coefficient of variation based image selective segmentation model

$$\min_{\phi,c_1,c_2}F_\epsilon(\phi,c_1,c_2)=\mu\int_\Omega d(x,y)g(|\nabla u|)\delta_\epsilon(\phi)|\nabla\phi|\,dx\,dy + \lambda_1\int_\Omega\frac{(u_0(x,y)-c_1)^2}{c_1^2}H_\epsilon(\phi)\,dx\,dy + \lambda_2\int_\Omega\frac{(u_0(x,y)-c_2)^2}{c_2^2}(1-H_\epsilon(\phi))\,dx\,dy,$$

where $d(x,y)$ denotes a metric function, used for selective

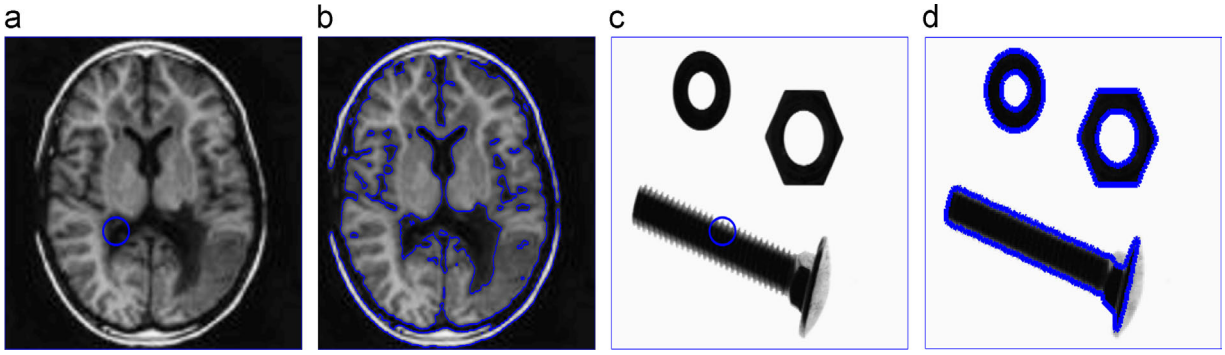

Fig. 1. Detection of edges by the CV model for images having regions/objects of varying/inhomogeneous intensities. (a) Original medical image with initial contour; (b) detection by the CV model; (c) original hardware image with initial contour; (d) detection by the CV model. Clearly some prominent edges are correctly identified but the objects are not identified correctly.

segmentation, and g is an edge detection function e.g. for some $p \geq 1$ and a Gaussian function $G_\sigma(x,y)$

$$g(|\nabla u_0(x,y)|) = \frac{1}{1+|\nabla G_\sigma(x,y) * u_0(x,y)|^p}.$$

This model was able to capture objects of interest in examples where the TV model failed. More examples can be found later in this paper.

2.2. The local Chan–Vese model (LCV)

To extend the CV model to deal with intensity inhomogeneity, Wang et al. [20] proposed a model by incorporating the following new local statistical fitting terms, $\int_{inside(\Gamma)}(u_0^* - u_0 - d_1)^2\,dx\,dy + \int_{out(\Gamma)}(u_0^* - u_0 - d_2)^2\,dx\,dy$ where $u_0^*(x,y) = g_k * u_0(x,y)$ is the smoothed version of the image u_0. The local Chan–Vese (LCV) energy functional in level set formulation is given by

$$\begin{aligned} F_\epsilon(\phi, c_1, c_2, d_1, d_2) = {} & \mu \int_\Omega \delta_\epsilon(\phi)|\nabla\phi|\,dx\,dy + \int_\Omega \frac{1}{2}(|\nabla\phi|-1)^2\,dx\,dy \\ & + \lambda_1 \int_\Omega (u_0 - c_1)^2 H_\epsilon(\phi)\,dx\,dy \\ & + \lambda_1 \int_\Omega (u_0 - c_2)^2 (1 - H_\epsilon(\phi))\,dx\,dy \\ & + \lambda_2 \int_\Omega (u_0^* - u_0 - d_1)^2 H_\epsilon(\phi)\,dx\,dy \\ & + \lambda_2 \int_\Omega (u_0^* - u_0 - d_2)^2 (1 - H_\epsilon(\phi))\,dx\,dy, \end{aligned} \tag{6}$$

where positive constants μ, λ_1, λ_2 are used for assigning different weights and g_k is an averaging convolution operator of window of size $k \times k$. Using $u_0^*(x,y)$ is the usual trick to deal with noise in u_0 (but at the expense of imprecise boundaries).

The first regularizer term $\int_\Omega \delta_\epsilon(\phi)|\nabla\phi|\,dx\,dy$ of the energy functional given in (6) helps to maintain the smoothness of the active curve. The second term is a metric which keeps the function ϕ close to a signed distance function in Ω. The global fitting term $\int_\Omega (u_0 - c_1)^2 H_\epsilon(\phi)\,dx\,dy + \int_\Omega (u_0 - c_2)^2 (1 - H_\epsilon(\phi))\,dx\,dy$ guides the active contour to capture the main structure of objects/regions of image u_0. The local term $\int_\Omega (u_0^* - u_0 - d_1)^2 H_\epsilon(\phi)\,dx\,dy + \int_\Omega (u_0^* - u_0 - d_2)^2 (1 - H_\epsilon(\phi))\,dx\,dy$ assists the detection of small and valuable details.

Minimization of $F_\epsilon(\phi, c_1, c_2, d_1, d_2)$ leads to the following solutions:

$$c_1(\phi) = \frac{\int_\Omega u_0(x,y) H_\epsilon(\phi)\,dx\,dy}{\int_\Omega H_\epsilon(\phi)\,dx\,dy}, \quad c_2(\phi) = \frac{\int_\Omega u_0(x,y)(1 - H_\epsilon(\phi))\,dx\,dy}{\int_\Omega (1 - H_\epsilon(\phi))\,dx\,dy},$$

$$d_1(\phi) = \frac{\int_\Omega (u_0^*(x,y) - u_0) H_\epsilon(\phi)\,dx\,dy}{\int_\Omega H_\epsilon(\phi)\,dx\,dy},$$

$$d_2(\phi) = \frac{\int_\Omega (u_0^*(x,y) - u_0)(1 - H_\epsilon(\phi))\,dx\,dy}{\int_\Omega (1 - H_\epsilon(\phi))\,dx\,dy},$$

and, with $\phi(x,y,t) = \phi_0(x,y,0)$,

$$\begin{aligned} \frac{\partial\phi}{\partial t} = {} & \delta_\epsilon(\phi)\Big[-\lambda_1(u_0 - c_1)^2 - \lambda_2(u_0^* - u_0 - d_1)^2 \\ & + \lambda_1(u_0 - c_2)^2 + \lambda_2(u_0^* - u_0 - d_2)^2\Big] \\ & + \left[\mu\delta_\epsilon(\phi)\nabla.\left(\frac{\nabla\phi}{|\nabla\phi|}\right) + \left(\nabla^2\phi - \nabla.\frac{\nabla\phi}{|\nabla\phi|}\right)\right] \quad \text{in } \Omega. \end{aligned} \tag{7}$$

In contrast with CV model, the LCV model works well in many examples with image inhomogeneity and low level noise [20]. The LCV model captures minute details and detects objects/regions with intensity inhomogeneity better than the CV model. However for images with high level noise, the LCV model may have to compromise between retaining noise as objects and keeping valuable minute details; see Figs. 2 and 3 where the model fails.

2.3. Fast global minimization of the active contour/snake model

To enhance the CV model for the images in which the contrast between the background and objects of interest is low, Bresson et al. [3] proposed a fast global minimization model (FGM) by combining the CV model with a snake model in a global minimization framework. Two new ideas are introduced. First, the usual length term $length(\Gamma)$ in a CV model is replaced by a weighted length. Second, the new variable $u = H(\phi)$ is introduced to define a convex function but the functional is not yet convex due to $u \in \{0,1\}$. Then a constraint on u such that $u \in [0,1]$ is adopted to derive a convex functional. That is, they first reformulate the following minimization functional

$$F(u = 1_{\Omega_c}, c_1, c_2, \lambda) = \int_C g\,ds + \lambda \int_\Omega \Big((u_0 - c_1)^2 - (u_0 - c_2)^2\Big) 1_{\Omega_c}\,dx\,dy \tag{8}$$

as a convex functional for u and then solve the new variational problem

$$\min_{u,v}\left\{\int_\Omega g|\nabla u|\,dx\,dy + \frac{1}{2\theta}\|u - v\|^2 + \int_\Omega \Big[\lambda\Big((u_0 - c_1)^2 - (u_0 - c_2)^2\Big)v + \alpha\nu(v)\Big]\,dx\,dy\right\}$$

where $g = g(|\nabla u_0|)$, 1_{Ω_c} denotes the characteristic function and $\nu(\xi) = \max\{0, 2|\xi - 1/2| - 1\}$ helps to impose $0 \leq u \leq 1$. Equipped with an edge detector function and image data fidelity terms, this model is transformed to global minimization framework and, based on the dual formulation, a fast segmentation algorithm is derived. Although this model [3] enhancing the CV model gives better results than the CV model in many examples, it shares some of the weakness of the CV model especially in locating edges according to intensities rather than finding objects.

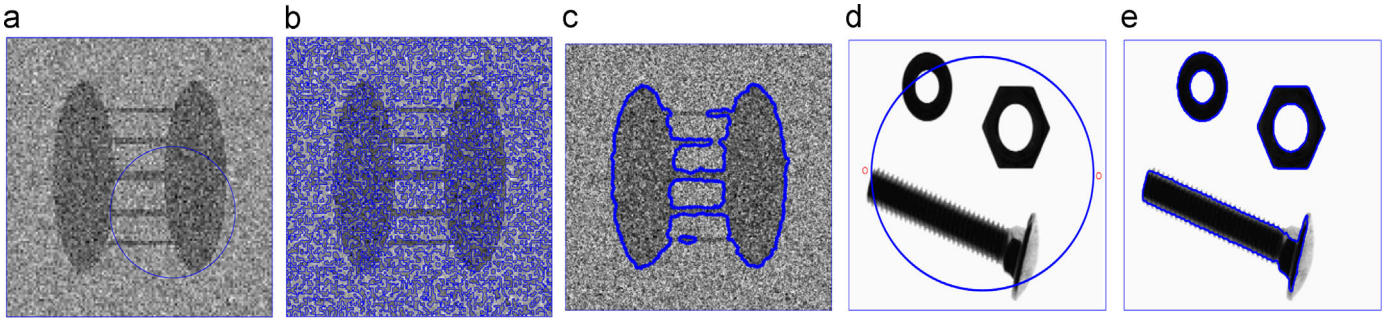

Fig. 2. Strong noise can reduce the effectiveness of the LCV model. (a) Synthetic noisy image with initial contour; (b) over detection by the LCV model when the local term is turned on; (c) under detection by the LCV model when the local term is turned off; (d) hardware image with initial contour; (d) detection by the COV model.

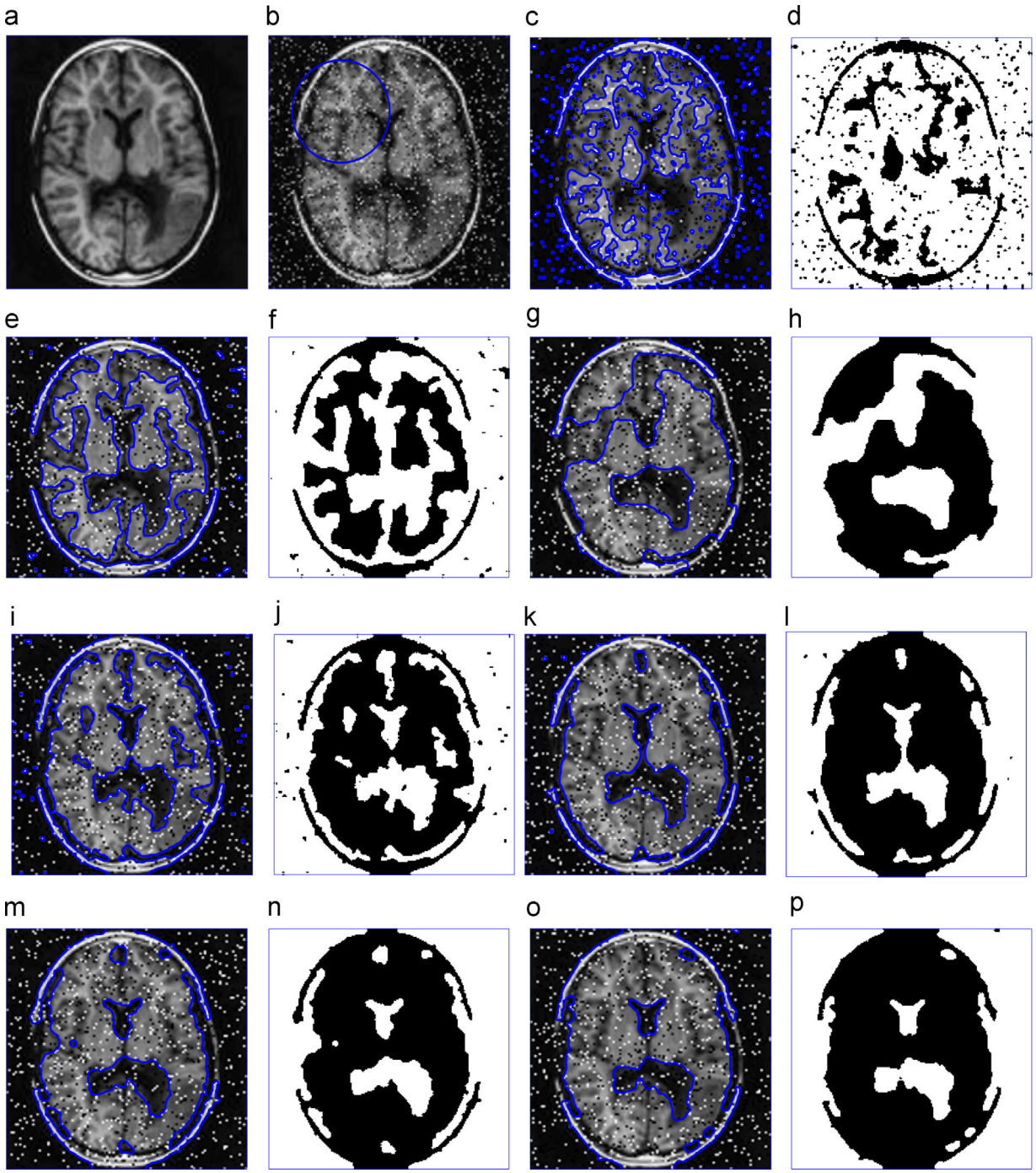

Fig. 3. (a) Original image. (b) Corrupted image. (c) 0.1×255^2, 0.1, 1. (d) Segmented result. (e) 0.2×255^2, 0.1, 1. (f) Segmented result. (g) 0.3×255^2, 0.1, 1. (h) Segmented result. (i) 0.5×255^2, 1, 1. (j) Segmented result. (k) 0.6×255^2, 1, 1. (l) Segmented result. (m) 0.7×255^2, 1, 1. (n) Initial contour. (o) 0.3×255^2, 1, 0.1. (p) Segmented result. Experimental tests of the LCV model, in segmenting a noisy image corrupted with salt & pepper noise with $p = 0.1$, reveal that LCV can avoid noise but it losses local information as well. Moreover, LCV consider noise as an object, when minute details in an image are important to be detected. For each test, parameters μ, λ_1, and λ_2 are respectively given, $size(u_0) = 200 \times 200$ and number of iterations are 3000.

The FGM model (8) works well for images having constant intensity regions; if the number of such constants is more than 2, a multiphase version of it is required. However if an object contains inhomogeneous intensities or two constant intensities, both the CV and the FGM or their multiphase versions cannot segment such objects. The failure of the FGM model can be seen in Fig. 4 where it fails the first test in Fig. 4(a) and (b) (unable to capture completely the screw) due to inhomogeneous intensities and it fails the second test in Fig. 4 (c) and (d) (unable to pick the complete object) due to strong noise. Similarly, for a third example, Fig. 5 reveals that the FGM model may capture some objects of a noisy image but lose other minute details.

3. A new segmentation model and its solution by operator splitting

In this section, we first discuss some motivations behind our model to present, and then give a solution method based on

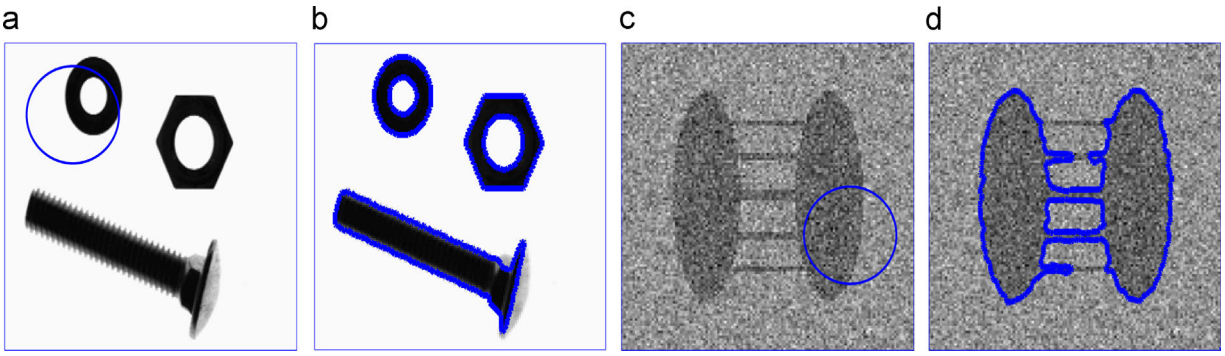

Fig. 4. Experimental tests of the FGM model on image having inhomogeneous intensity and/or noise. (a) Original hardware image; (b) detection by the FGM model; (c) synthetic noisy image; (d) detection by the FGM model. Clearly the first result (b) identified the edges correctly but not the object, while the second result (d) suggests that the problem is too challenging for FGM.

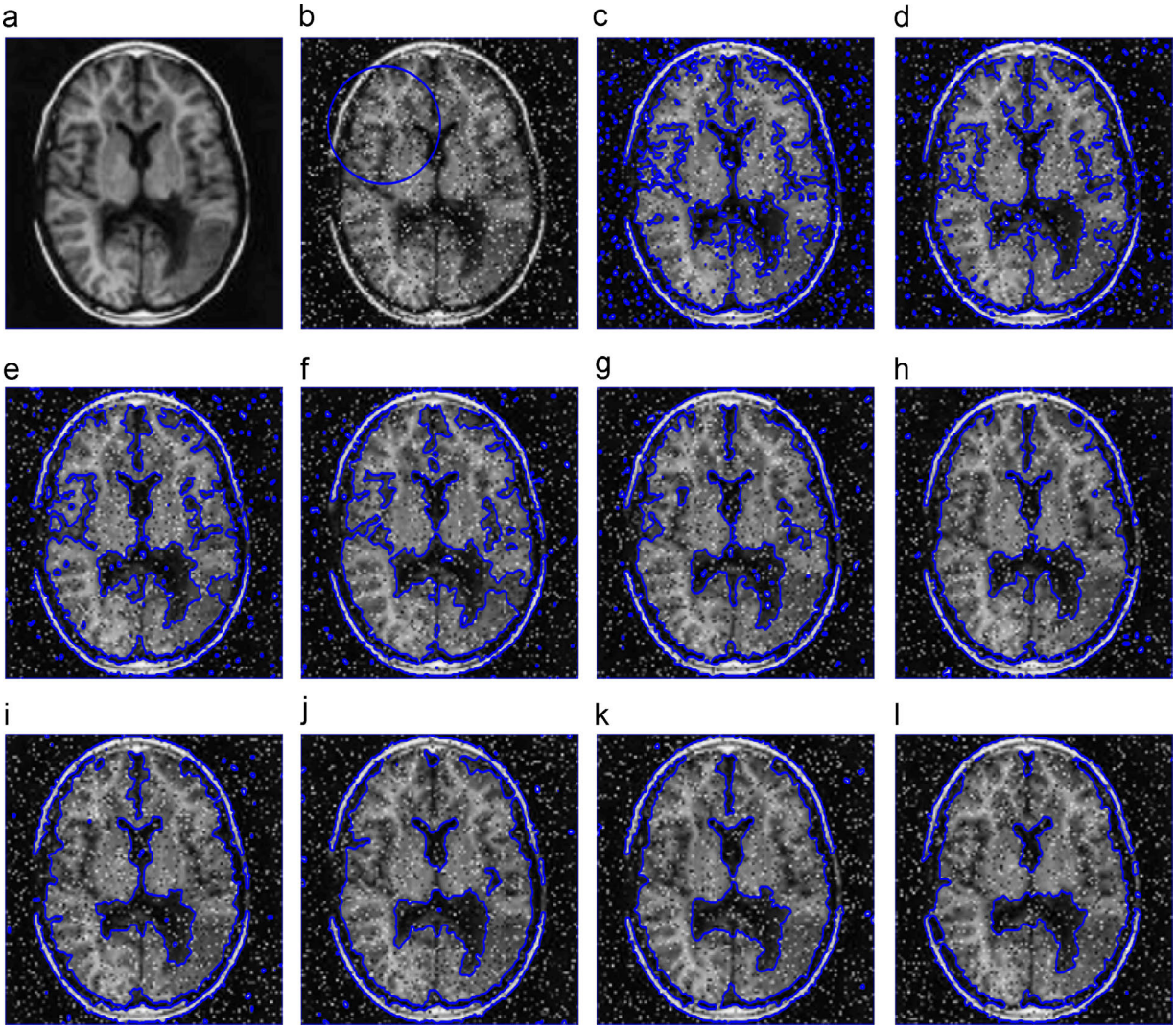

Fig. 5. (a) Original image. (b) Corrupted image. (c) $\theta=5$. (d) $\theta=10$. (e) $\theta=15$. (f) $\theta=20$. (g) $\theta=25$. (h) $\theta=30$. (i) $\theta=35$. (j) $\theta=40$. (k) $\theta=45$. (l) $\theta=50$. Experimental tests using FGM model, in segmenting a noisy image corrupted with salt & pepper noise with $p=0.1$.

operator splitting. To segment images having regions/objects of inhomogeneous intensities and noise, the level set function (LSF) should be constrained and the fitting terms $\int_{\Omega}(u_0-c_1)^2 H_{\epsilon}(\phi)dx\,dy+\int_{\Omega}(u_0-c_2)^2(1-H_{\epsilon}(\phi))dx\,dy$ alone are insufficient.

We propose to employ both local and global image information to guide a LSF to capture minute details other than noise, and for complete detection of the global structure of objects in image u_0. Here the local image information helps to handle varying intensities in a region so that the complete region can be detected and the global image information works in alliance with local image information to capture important minute details other than noise. Also, the global image information is

responsible for detection of the global structures of objects in an image.

Motivation towards to the new model can be seen in Fig. 6. Original image u_0 is given, in Fig. 6(a), and in Fig. 6(b) the smooth version of the given image u_0^* is given. Clearly, u_0, u_0^* seem challenging to segment, as the edges are not that much prominent, while in the product image $u_0u_0^*$ given in Fig. 6(c) and the difference image $255-(u_0^*-u_0)$ given in Fig. 6(d) the edges are more prominent and is less challenging to segment. We also see that although local details in Fig. 6(c) have disappeared, the main and global structure is more prominent than u_0. Similarly, local and minute details are now more visible and prominent in Fig. 6(d). These observations lead us to design functionals capable to guide a LSF both locally and globally to capture accurately the desired edges/regions completely. Our new proposed model will make use of both $u_0u_0^*$ and $u_0^*-u_0$. This processing idea is similar to high pass filtering

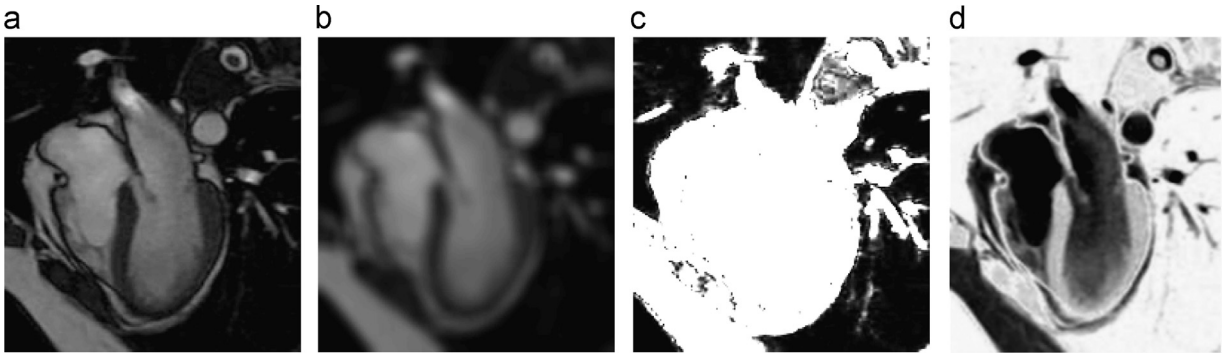

Fig. 6. Illustration of two related but different image functions $u_0u_0^*$ and $255-(u_0^*-u_0)$ for a new model: (a) the original image; (b) the smoothed image; (c) product $u_0u_0^*$ with enhanced global and subregion details; (d) difference image $255-(u_0^*-u_0)$ with edge and local details. Clearly using (d) alone without (c), as in LCV, appears insufficient for segmentation.

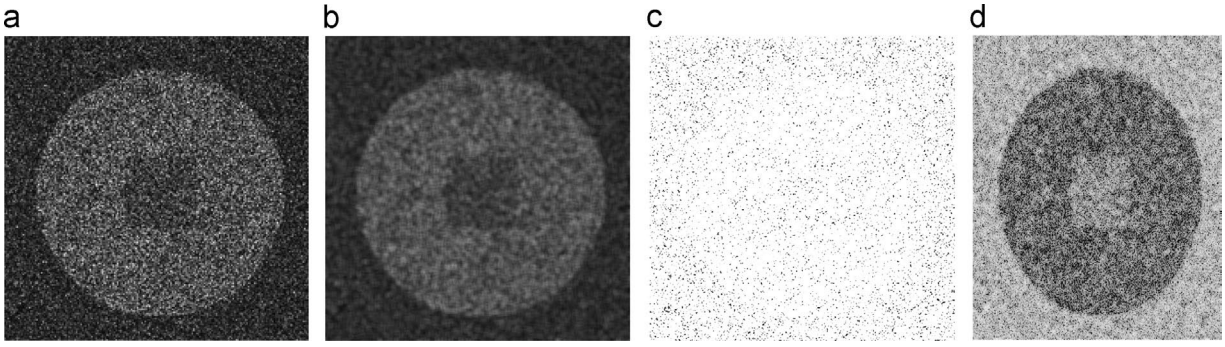

Fig. 7. Another illustration of two related but different image functions $u_0u_0^*$ and $255-(u_0^*-u_0)$ for a new model: (a) the original image with noise; (b) the smoothed image; (c) product $u_0u_0^*$ with enhanced global and object details; (d) difference image $255-(u_0^*-u_0)$ with edge and local details.

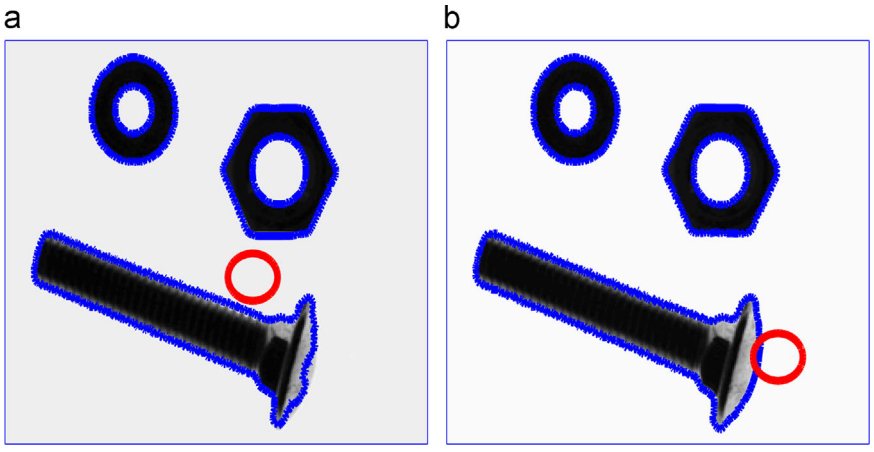

Fig. 8. Illustration of the non-convexity of the proposed energy functional. (a) An initial guess contour (circle) leads to incorrect segmentation; (b) another initial circle leads to correct segmentation.

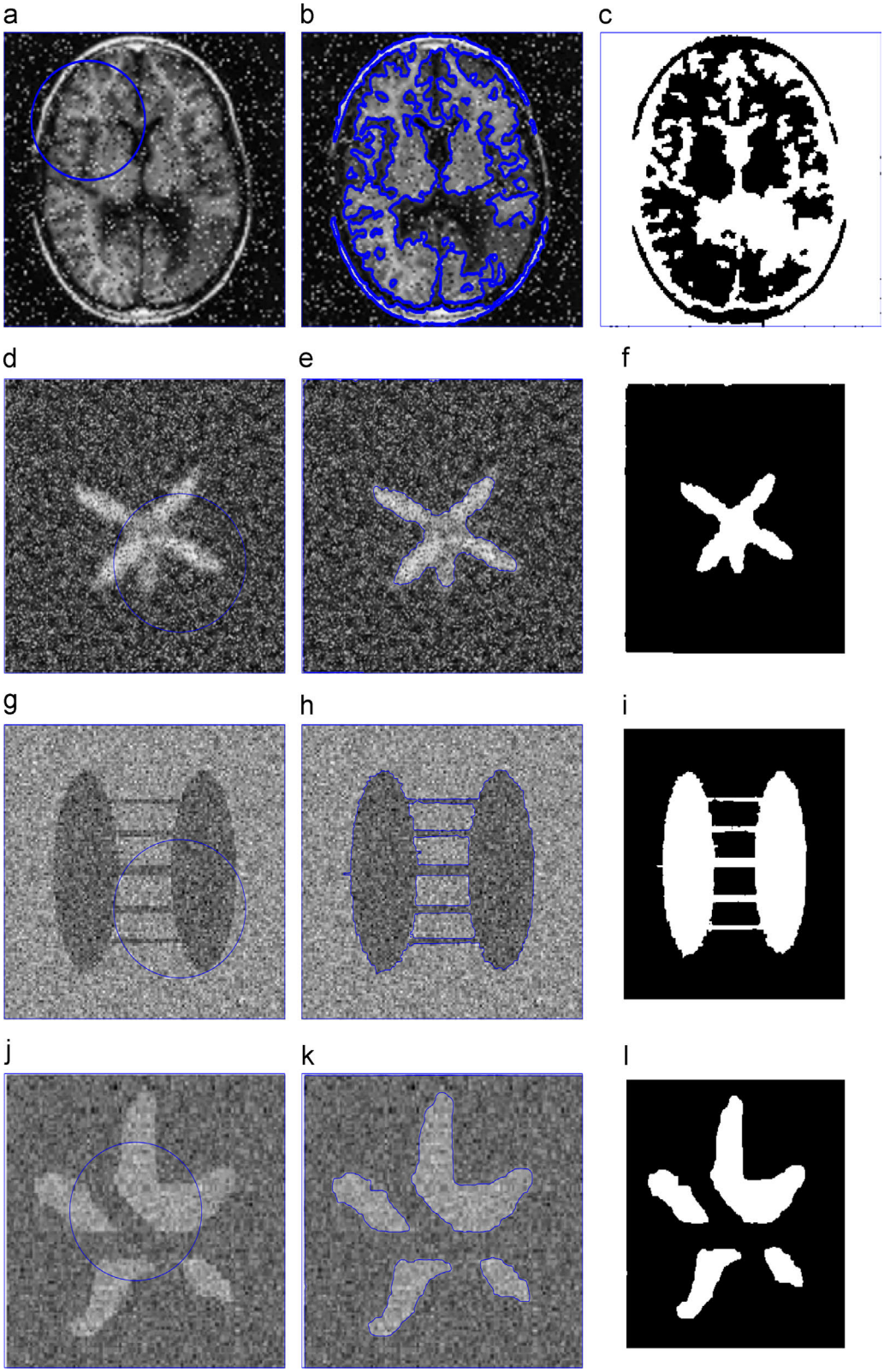

Fig. 9. (a) Initial contour. (b) 200 iterations. (c) Segmented result. (d) Initial contour. (e) 30 iterations. (f) Segmented result. (g) Initial contour. (h) 5 iterations. (i) Segmented result. (j) Initial contour. (k) 30 iterations. (l) Segmented result. The complete detection by the proposed DMD method on segmenting noisy images: (Row First) Parameters used are: $\lambda_1 = 0.3$, $\lambda_2 = 1$, $\mu = 5 \times 10^3 \times size(u_0)$, $\sigma_s = 30$, $\sigma_l = 15$; (row second) Parameters used are: $\lambda_1 = 1$, $\lambda_2 = 0.5$, $\mu = 5 \times 10^3 \times size(u_0)$, $\sigma_s = 20$, $\sigma_l = 30$; (row third) Parameters used are: $\lambda_1 = 1$, $\lambda_2 = 1$, $\mu = 2 \times 10^3 \times size(u_0)$, $\sigma_s = 40$, $\sigma_l = 30$; (row fourth) parameters used are: $\lambda_1 = 0.5$, $\lambda_2 = 1$, $\mu = 25 \times 10^2 \times size(u_0)$, $\sigma_s = 15$, $\sigma_l = 30$.

in frequency domain where high frequency components like edges and minute important details are boosted at the expense of the low-frequency components. The high-pass filtered image in Fig. 6 (d) contains only high frequency components.

In Fig. 7 another example is given. Original noisy image u_0 in given in Fig. 7(a), while the smoothed version of the image u_0^* is given in Fig. 7(b). The product image $u_0 u_0^*$ is given in Fig. 7 (c) and the difference image $255 - (u_0^* - u_0)$ is given in Fig. 7(d). It

can be seen that the object of interest is enhanced in Fig. 7 (c) and (d).

Based on the above discussion, for images with intensity inhomogeneity, the term $\int_{inside(\Gamma)}(u_0u_0^*-c_1)^2\,d\Omega$ is used instead of $\int_{inside(\Gamma)}(u_0-c_1)^2\,d\Omega$ and same for outside Γ. Thus, we propose the following new variational model for segmentation of images with intensity inhomogeneity

$$\min_{\Gamma,c_1,c_2,d_1,d_2}\{F(\Gamma,c_1,c_2,d_1,d_2)=\mu\ length(\Gamma)+\lambda_1F_1+\lambda_2F_2\}, \tag{9}$$

where

$$F_1=\int_{outside(\Gamma)}(u_0u_0^*-c_1)^2\,dx\,dy+\int_{inside(\Gamma)}(u_0u_0^*-c_2)^2\,dx\,dy,$$

$$F_2=\int_{outside(\Gamma)}(w^*-w-d_1)^2\,dx\,dy+\int_{inside(\Gamma)}(w^*-w-d_2)^2\,dx\,dy,$$

and c_1, c_2, d_1, d_2 are the average intensities of the difference image (w^*-w) and of $w=u_0u_0^*$ inside and outside Γ respectively. Our model is not of the CV type, though similar variational

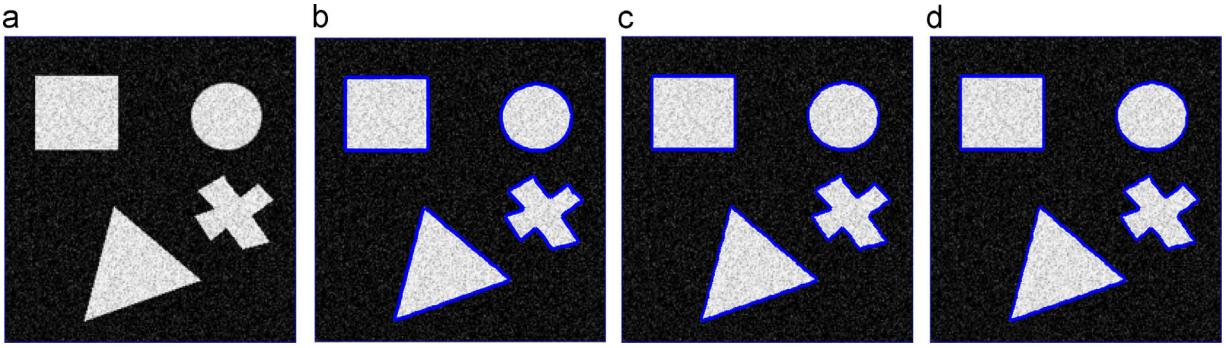

Fig. 10. (a) Given image. (b) LCV. (c) FGM. (d) DMD. Illustration of a simple noisy image and the performance of all the three models.

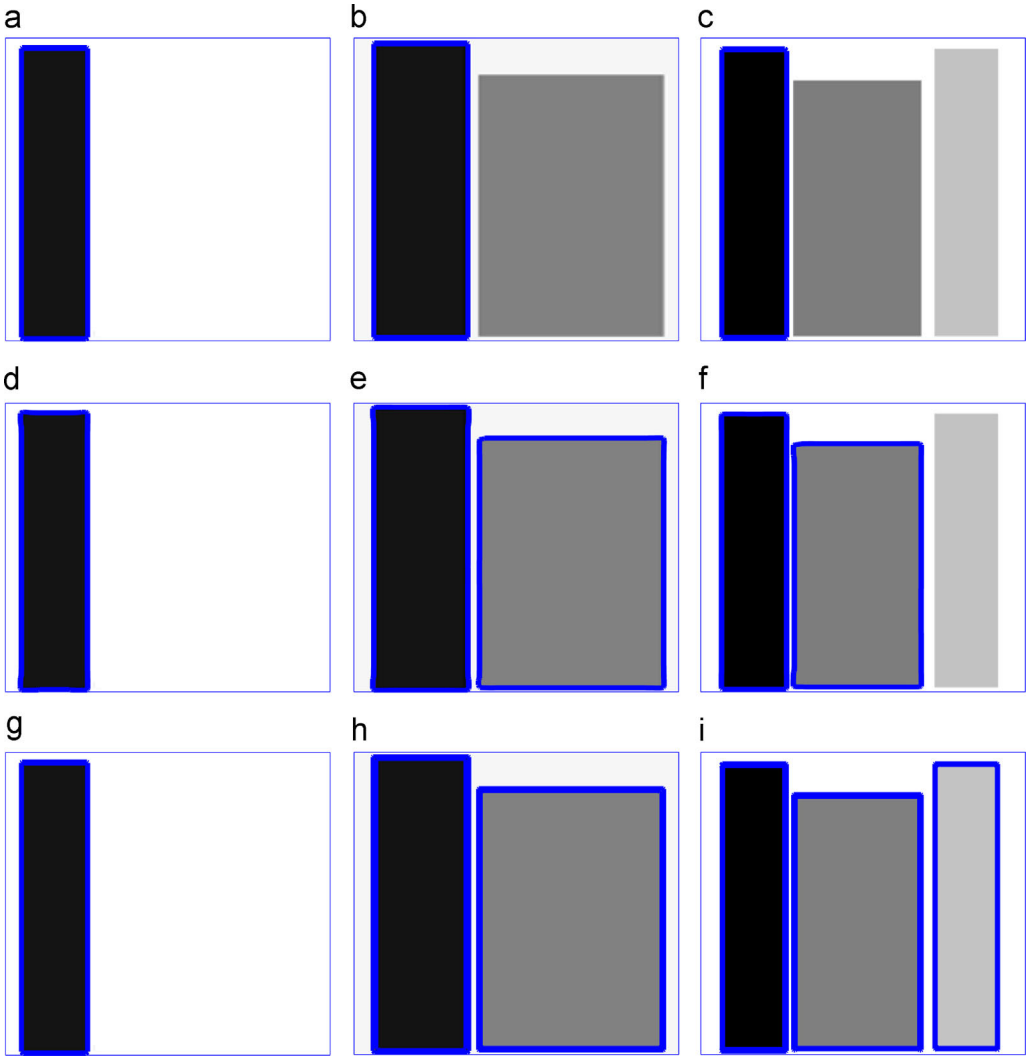

Fig. 11. (a) (FGM). (b) (FGM). (c) (FGM). (d) (LCV). (e) (LCV). (f) (LCV). (g) (DMD). (h) (DMD). (i) (DMD). Comparison 1 of three models for images of size 256 × 256: (Column 1) All the three models are working well; (Column 2) The LCV and DMD model are working well; (Column 3) Only the DMD model is working well.

framework is used.

In level set formulation we have the following minimization problem,

$$F(\phi, c_1, c_2, d_1, d_2) = \mu \int_\Omega \delta(\phi)|\nabla\phi|\ dx\ dy + \int_\Omega \left[\lambda_1(u_0 u_0^* - c_1)^2 + \lambda_2(w^* - w - d_1)^2\right] H(\phi)\ dx\ dy + \int_\Omega \left[\lambda_1(u_0 u_0^* - c_2)^2 + \lambda_2(w^* - w - d_2)^2\right] \times (1 - H(\phi))\ dx\ dy, \quad (10)$$

or its regularized form

$$F_\epsilon(\phi, c_1, c_2, d_1, d_2) = \mu \int_\Omega \delta_\epsilon(\phi)|\nabla\phi|\ dx\ dy + \int_\Omega \left[\lambda_1(u_0 u_0^* - c_1)^2 + \lambda_2(w^* - w - d_1)^2\right] H_\epsilon(\phi)\ dx\ dy + \int_\Omega \left[\lambda_1(u_0 u_0^* - c_2)^2 + \lambda_2(w^* - w - d_2)^2\right] (1 - H_\epsilon(\phi))\ dx\ dy,$$

where μ, λ_1 and λ_2 are positive constants used for assigning different weights, and H_ϵ is a regularized Heaviside function [1–3]. Keeping ϕ fixed and minimizing $F_\epsilon(\phi, c_1, c_2, d_1, d_2)$ with respect to c_1, c_2, d_1 and d_2 we have

$$c_1(\phi) = \frac{\int_\Omega u_0 u_0^* H_\epsilon(\phi)\ dx\ dy}{\int_\Omega H_\epsilon(\phi)\ dx\ dy}, c_2(\phi) = \frac{\int_\Omega u_0 u_0^* (1 - H_\epsilon(\phi))\ dx\ dy}{\int_\Omega (1 - H_\epsilon(\phi))\ dx\ dy},$$

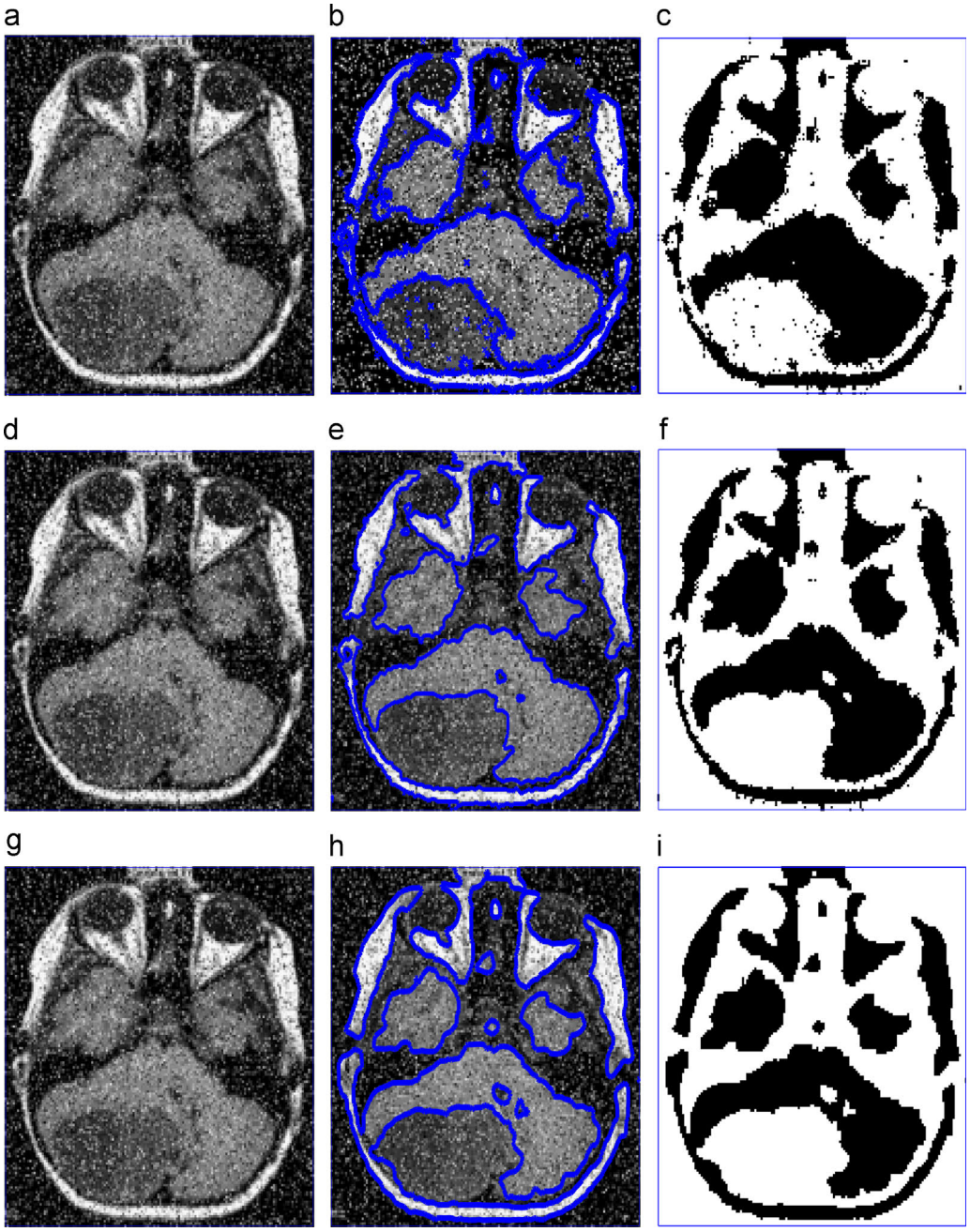

Fig. 12. (a) Given image. (b) 1000 iterations (LCV). (c) Segmented result. (d) Given image. (e) 10^4 iterations (FGM). (f) Segmented result. (g) Given image (h) 450 iterations (DMD). (i) Segmented result comparison 2 of three models in segmenting a noisy image of size 150×150: (first row) The performance of LCV model; (second row) The performance of FGM model; (row third) The performance of DMD model. Parameters used are: $\lambda_1 = 0$, $\lambda_2 = 1$, $\mu = 2 \times 10^3 \times 150^2$, $\sigma_s = 30$, $\sigma_l = 25$.

$$d_1(\phi)=\frac{\int_\Omega (w^*(x,y)-w)H_\epsilon(\phi)\,dx\,dy}{\int_\Omega H_\epsilon(\phi)\,dx\,dy},$$
$$d_2(\phi)=\frac{\int_\Omega (w^*(x,y)-w)(1-H_\epsilon(\phi))\,dx\,dy}{\int_\Omega (1-H_\epsilon(\phi))\,dx\,dy}.$$

Now keeping c_1, c_2, d_1 and d_2 fixed and minimizing F_ϵ with respect to ϕ yields the following Euler–Lagrange partial differential equation PDE) for ϕ

$$\delta_\epsilon(\phi)\left[\mu\,\mathrm{div}\left(\frac{\nabla\phi}{|\nabla\phi|}\right)+\lambda_1(u_0u_0^*-c_1)^2-\lambda_1(u_0u_0^*-c_2)^2+\lambda_2(w^*-w-d_1)^2-\lambda_2(w^*-w-d_2)^2\right]=0 \quad \text{in } \Omega, \tag{11}$$

where $\frac{\partial\phi}{\partial\vec{n}}\Big|_{\partial\Omega}=0$, $\vec{n}$ is an exterior unit normal to the boundary $\partial\Omega$. Since our model involves *D*ouble fitting terms of *M*ultiplicative and *D*ifference images, we shall name it as DMD model. The above PDE may be considered as a steady state solution of the following evolution equation:

$$\frac{\partial\phi}{\partial t}=\delta_\epsilon(\phi)\left[\mu\nabla.\left(\frac{\nabla\phi}{|\nabla\phi|}\right)+\lambda_1(u_0u_0^*-c_1)^2-\lambda_1(u_0u_0^*-c_2)^2+\lambda_2(w^*-w-d_1)^2-\lambda_2(w^*-w-d_2)^2\right],$$

$$\phi(x,y,t)=\phi_0(x,y,0)\ \text{in}\ \Omega. \tag{12}$$

An additive operator splitting method: We shall use an Additive Operator Splitting (AOS) method to solve (12), as done in [21–24], which is unconditionally stable. Defining $W=1/|\nabla\phi|$, we write Eq. (12) in the form:

$$\frac{\partial\phi}{\partial t}=\mu\delta_\epsilon(\phi)\nabla(W\nabla\phi)+f=\mu\delta_\epsilon(\phi)\big(\partial_x(W\partial_x\phi)+\partial_y(W\partial_y\phi)\big)+f.$$

The AOS scheme [21,22] splits the 2-dimensional spatial operator into a sum of two one-dimensional ones, solved separately before merging. By a finite difference discretization, we consider first the one-dimensional problem in the x-direction

$$\phi_{i,j}^{k+1}=\phi_{i,j}^{k}+\mu\Delta t\left(c_1\phi_{i+1,j}^{n+1}-c_2\phi_{i,j}^{n+1}+c_3\phi_{i-1,j}^{n+1}\right)+f_i, \tag{13}$$

where $c_1=\delta_\epsilon(\phi)^{\frac{W_{i,j}^k+W_{i+1,j}^k}{2}}$, $c_2=\delta_\epsilon(\phi)^{\frac{W_{i-1,j}^k+2W_{i,j}^k+W_{i+1,j}^k}{2}}$, $c_3=\delta_\epsilon(\phi)^{\frac{W_{i,j}^k+W_{i-1,j}^k}{2}}$. After we solve the system of Eq. (13) in the x-direction, we then solve a similar system in y-direction before averaging the two solutions

$$(I-2\Delta tA_l(\Phi^k))\Phi_l^{k+1}=\Phi^k+f^k \quad \text{for } l=1,2, \text{ and } \Phi^{k+1}=\frac{1}{2}\sum_{l=1}^{2}\Phi_l^{k+1},$$

where I is the identity matrix and A_l for $l=1,2$ a tridiagonal matrix.

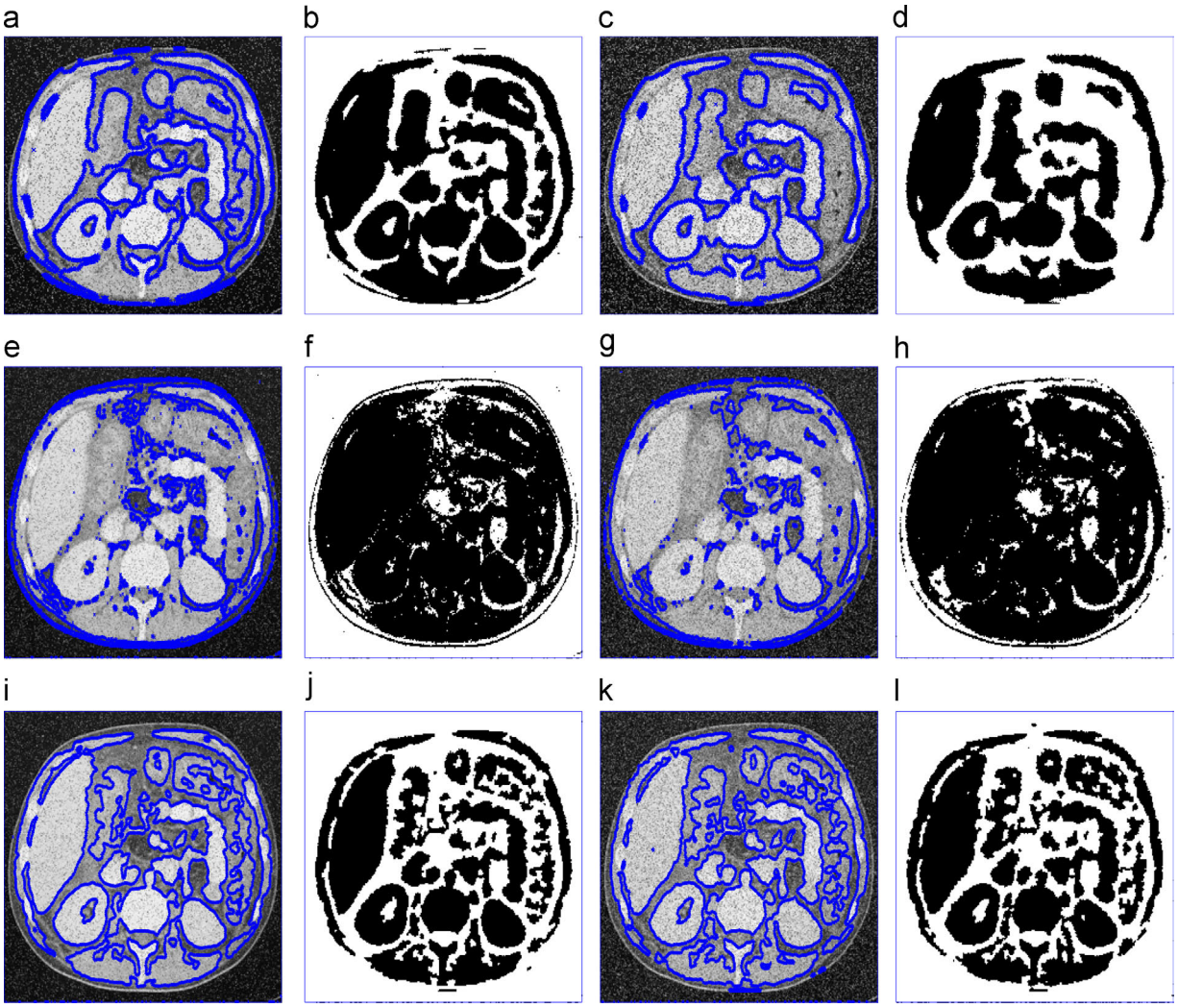

Fig. 13. (a) LCV ($p=0.1$). (b) Segmented result. (c) LCV ($p=0.2$). (d) Segmented result. (e) FGM ($p=0.1$). (f) Segmented result. (g) FGM ($p=0.2$). (h) Segmented result. (i) DMD ($p=0.1$). (j) Segmented result. (k) DMD ($p=0.2$). (l) Segmented result. Comparison 3 of three models in segmenting a given abdominal image of size 256×256, corrupted with mild salt & pepper noise with noise level p, reveals that the DMD performs better than the LCV and FGM model.

4. The new model in fast global minimization framework

The proposed model is nonconvex and may stuck at local minima. This behavior of the model can be seen in Fig. 8, where two different initial guesses lead to two different segmentation results. As a consequence, the initial guess becomes very important for satisfactory results [25–27].

The non-convexity of the proposed functional can be handled by using fast global minimization framework. The proposed model in global minimization framework reformulates the non-convex functional (with non-convexity due to 1_{Ω_1})

$$F(1_{\Omega_1}, c_1, c_2, \lambda) = \int_\Gamma g\, ds + \lambda_1 \int_\Omega \left((u_0 u_0^* - c_1)^2 - (u_0 u_0^* - c_2)^2\right) 1_{\Omega_1}\, dx\, dy$$

$$+ \lambda_2 \int_\Omega \left((w^* - w - d_1)^2 - (w^* - w - d_2)^2\right) 1_{\Omega_1}\, dx\, dy,$$

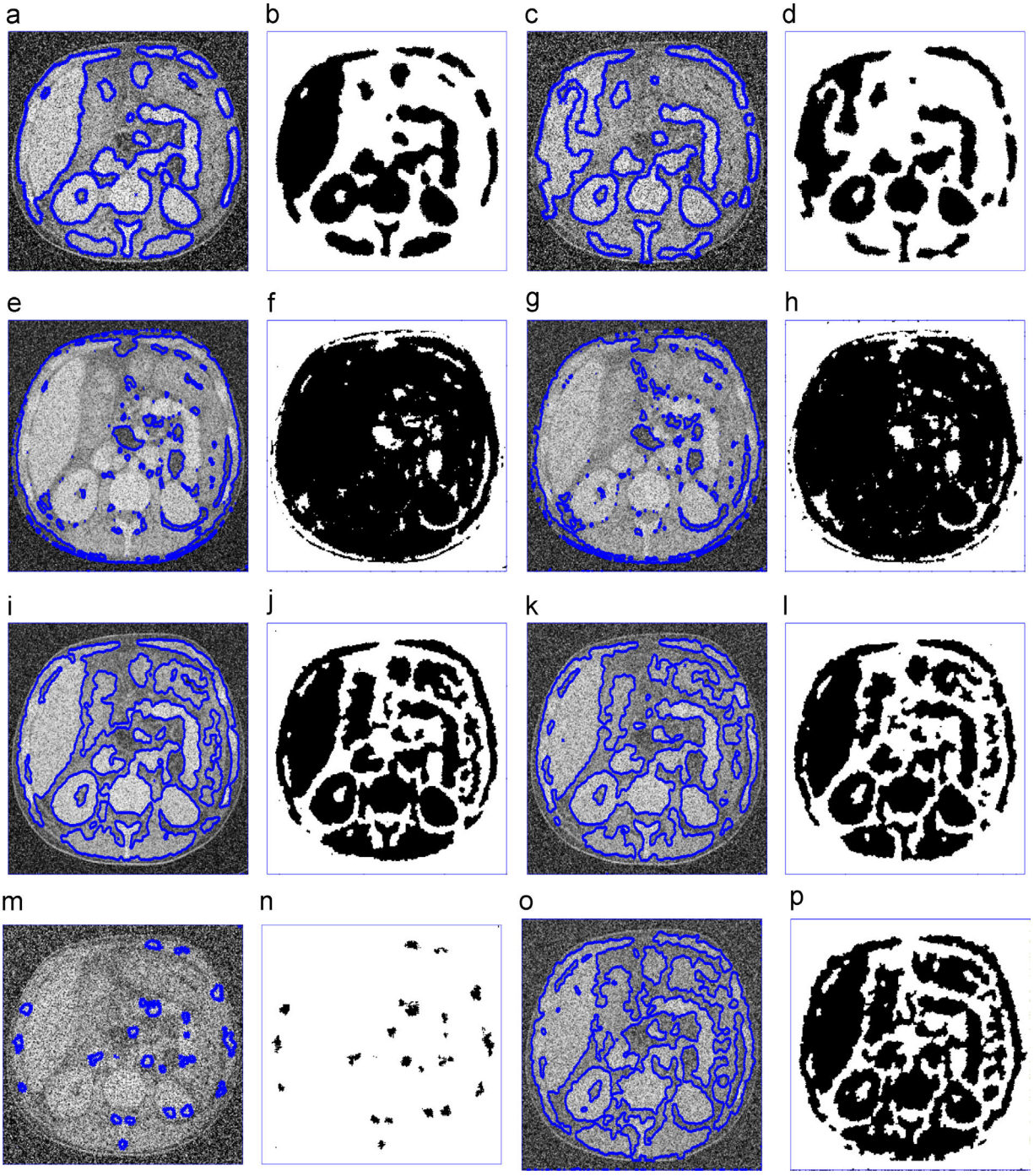

Fig. 14. (a) LCV ($p = 0.3$). (b) Segmented result. (c) LCV ($p = 0.4$). (d) Segmented result. (e) FGM ($p = 0.3$). (f) Segmented result. (g) FGM ($p = 0.4$). (h) Segmented result. (i) DMD ($p = 0.3$). (j) Segmented result. (k) DMD ($p = 0.4$). (l) Segmented result. (m) LCV ($p = 0.5$). (n) Segmented result. (o) DMD ($p = 0.5$). (p) Segmented result. Comparison 4 of three models for segmenting another abdominal image corrupted with strong salt & pepper noise with noise level p. Again the DMD performs better than the LCV and the FGM model. $size(u_0) = 256 \times 256$.

as a convex functional

$$F(u,c_1,c_2,\lambda)=\int_\Gamma g\,ds+\lambda_1\int_\Omega\left((u_0u_0^*-c_1)^2-(u_0u_0^*-c_2)^2\right)u\,dx\,dy$$
$$+\lambda_2\int_\Omega\left((w^*-w-d_1)^2-(w^*-w-d_2)^2\right)u\,dx\,dy,$$

where $\Omega_1=inside(\Omega)$, $1_{\Omega_1}(x,y)=H(\phi(x,y))=1$ if $(x,y)\in\Omega_1$ and $=0$ if $(x,y)\notin\Omega_1, u\in[0,1]$. The above model is further solved by a splitting method by introducing v to lead to the following variational problem:

$$\min_{u,v}\left\{\int_\Omega g|\nabla u|\,dx\,dy+\frac{1}{2\theta}\|u-v\|^2+\int_\Omega[f+\alpha\nu(v)]\,dx\,dy\right\}\qquad(14)$$

where $w=u_0u_0^*$, $\nu(v)$ is as in (8) and

$$f=\lambda_1\left[(u_0u_0^*-c_1)^2-(u_0u_0^*-c_1)^2\right]+\lambda_2\left[(w^*-w-d_1)^2-(w^*-w-d_2)^2\right].$$

The above convex formulation of the energy functional empowers convergence towards global minimum. The solution of the minimization problem (14) can be similarly done to [3], as summarized below:

Algorithm to solve (14)

Step 1: Set up an initial contour for u with 1 in a region (e.g. square) and 0 elsewhere. Compute $w=u_0u_0^*$.
Step 2: Solve (14) to update c_1,c_2,d_1,d_2.
Step 3: Solve (14) with respect to u (which is similar to a denoising problem).
Step 4: Update $\nu(v)$ analytically; see [3].
Step 5: Check the convergence of u: if converged, stop; else return to Step 2.
Step 6: Obtain the segmented domain Ω_1 from $u\le 0.5$.

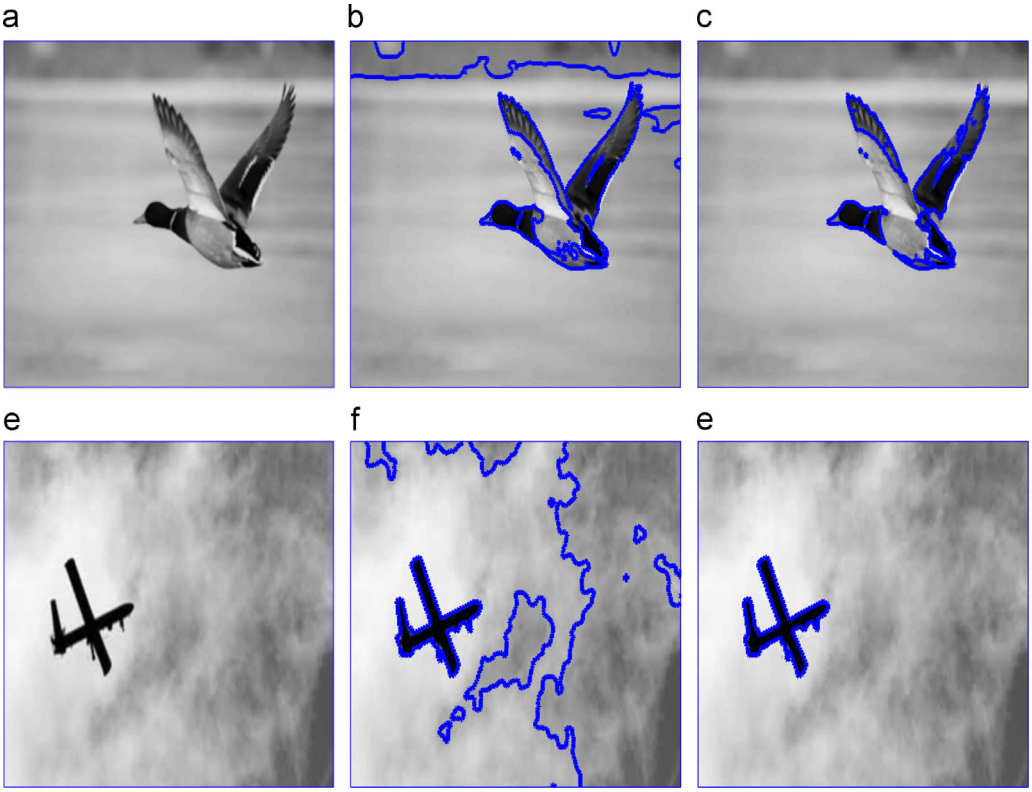

Fig. 15. (a) Original image. (b) FGM. (c) *DMD*. (d) Original image. (e) FGM. (f) *DMD*. Comparison 5 of the DMD and the FGM model on clutter background images.

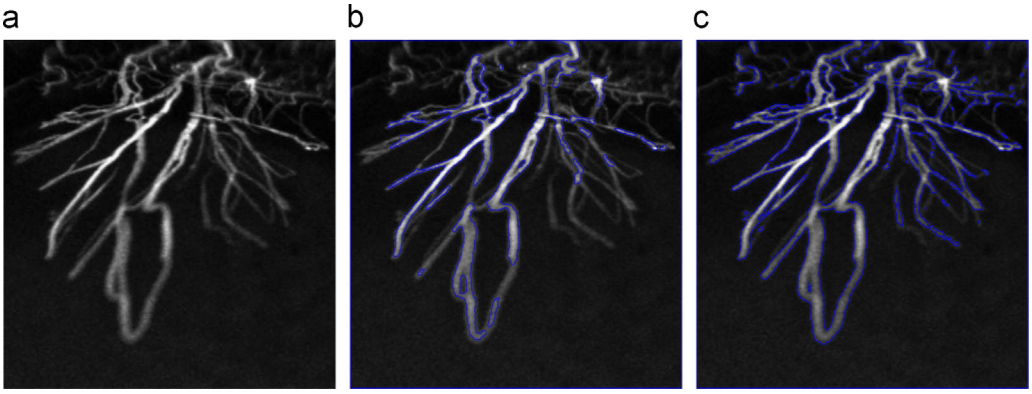

Fig. 16. Comparison 6 of our DMD method with the FGM method on segmenting a real cornea image: (a) Original image of size 256×256; (b) detection by the FGM method (5000 iterations); (c) detection by the DMD method (5 iterations). For the DMD method, $\lambda_1=0.1$, $\lambda_2=1$, $\mu=size(u_0)/10^6$, $\sigma_s=1$, $\sigma_l=30$. Clearly, the DMD method performs better.

5. Experimental results

In this section we give experimental justification of our proposed model and its comparisons with the LCV [20] and the FGM [3]. These experiments show that our new proposed model is robust in segmentation of objects in a range of images that have intensity inhomogeneity, multiphases, noise and low contrast or do not have piecewise constant intensities, while the existing models work well problems having homogeneous intensities.

(1) *Segmentation results of the DMD model for noisy images*: In Fig. 9, the DMD model is tested on a set of noisy images. It clearly reveals good segmentation results of the DMD model, both in terms of detection quality and the number of AOS iterations.

(2) *All models work well for an ideal image*: In Figs. 10 and 11, experimental tests Fig. 10(b)–(d), Fig. 11(a), (d), (g) demonstrate the good performance of all three models and shows that all work well on this simple image as exhibited. Onward experiments will reveal a different story for more challenging examples.

(3) *Multiphase problems*: Multi-phases refer to the distribution of intensities in an image having a few clearly identifiable clusters (either visibly or from its histogram); each cluster alone is traditionally called a phase but a phase may often represent only part of an object. In Fig. Fig. 11 the three models are tested on a multiphase type synthetic image. It can be observed that the proposed DMD model detects all the regions of multi-intensities and, in contrast, the LCV in Fig. 11(f) and the FGM model in Fig. 11(b) and (c) lead to unsuccessful results. Here each intensity represents an object, a multiphase model for piecewise constant intensities such as [26,27] should be able to segment this image. That is, it is not surprising that the two phase FGM cannot segment all objects.

(4) *Comparisons of three models for noisy images*: In Figs. 12–14, the three models (the LCV, the FGM and the DMD) are tested on noisy medical images. Fig. 12 shows test results on a brain medical image corrupted with salt and pepper noise. On one hand, the LCV model fails by classifying noise as valuable details whereas the FGM model produces undesirable rough edges as a result. On the

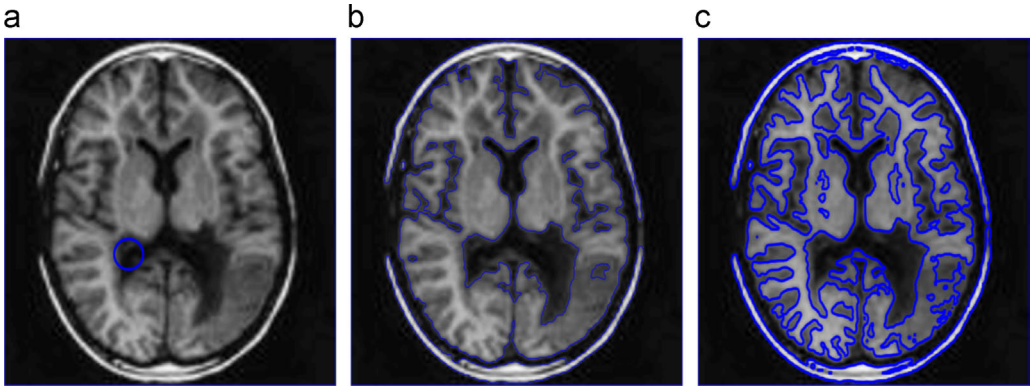

Fig. 17. Comparison 7 of our DMD method with the FGM method on a given medical brain image which has regions of inhomogeneous intensities. (a) Original image of size 256×256; (b) detection of the FGM method; (c) complete detection of the DMD method. Here $\lambda_1 = 0.1$, $\lambda_2 = 1$, $\mu = size(u_0)/10$, $\sigma_s = 7$, $\sigma_l = 35$.

Table 1
Efficiency comparison of the LCV, FGM and the proposed DMD models' algorithms.

Image size	LCV		*FGM*		*DMD*	
	Iter	CPU	Iter	CPU	Iter	CPU
400×400	16	3	5	2	4	1
800×800	18	13	8	4	6	2
1600×1600	20	56	21	16	15	10
2400×2400	23	157	40	58	33	46

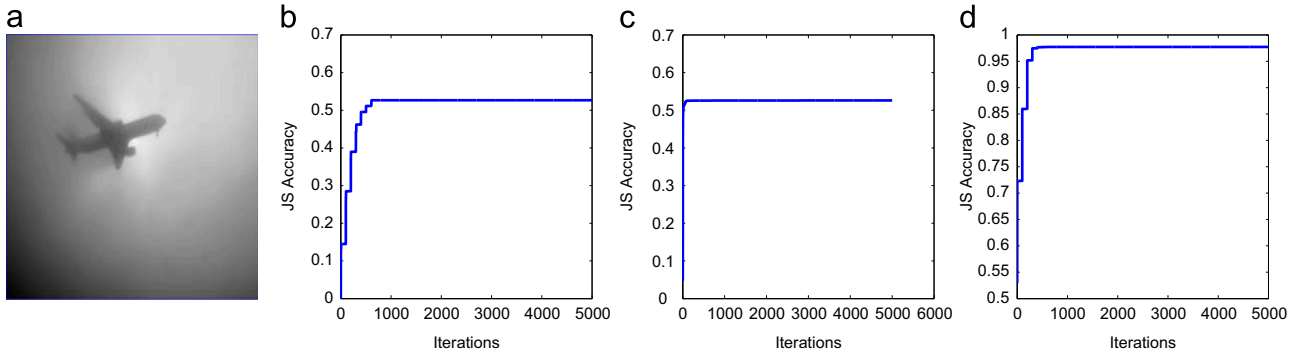

Fig. 18. Comparison 8 of three models in segmenting a real world image: (a) Original image of size 256×256; (b) result of the FGM method (JS=0.52); (c) result of the LCV method (JS=0.51); (d) result of the DMD method (JS=0.97).

other hand the proposed DMD model gives the best result. Similarly Figs. 13 and 14 show the performance of the three models on a real abdominal medical image with different levels of salt and pepper noise. It can be easily observed that our model successfully handles noise levels and produces the desired segmentation result.

Fig. 15 displays performance of the FGM and the proposed DMD model on images with cluttered background. The experimental tests validate that the new DMD model successfully tackles the clutter background and captures the desired objects. Fig. 16 displays a real cornea image and compares the performance of the DMD and FGM models. It can be easily observed that the proposed DMD model performs better than the FGM model. Next, a medical brain image is tested in Fig. 17, comparing the quality of segmentation and robustness of the FGM with the proposed DMD model: the test results can be interpreted that the quality of segmentation of the FGM model for the medical brain image is not good as the DMD; the reason is that the image with intensity inhomogeneity is too challenging for the FGM.

(5) *Solution efficiency*: Finally, using the synthetic noisy image from Fig. 10, we compare the three models' algorithms for efficiency and show the results in Table 1: the terms used in the headings of Table 1 have the following meanings:

Size: the size of given image $m \times n$.

Iter: the number of iterations used to get the required result.

CPU: the CPU time in seconds required to perform these iterations. The computation is carried out using MATLAB 7.11.0, in Windows 8 environment on a personal computer with 2.53 GHz Intel Core i3 and 2GB RAM. From Table 1, it can be observed that the proposed AOS method for our DMD model is efficient than the LCV and FGM implementations in terms of CPU time.

6. Quantitative analysis of energies

To test quantitatively the accuracy of the models we implement the Jaccard Similarity (JS) on simple two phase images and on

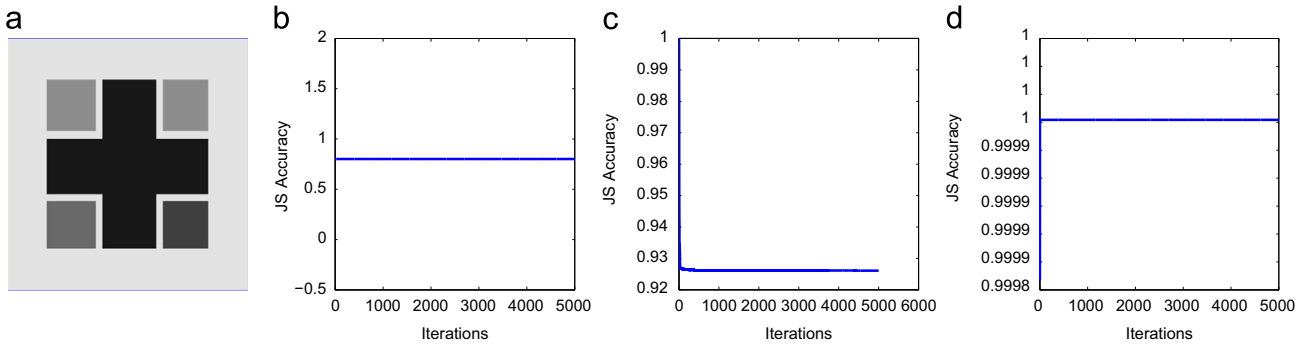

Fig. 19. Comparison 9 of three models in segmenting a synthetic multiphase type image: (a) Original image of size 256 × 256; (b) result of the FGM method (JS=0.8); (c) result of the LCV method (JS=0.92); (d) result of the DMD method (JS=1).

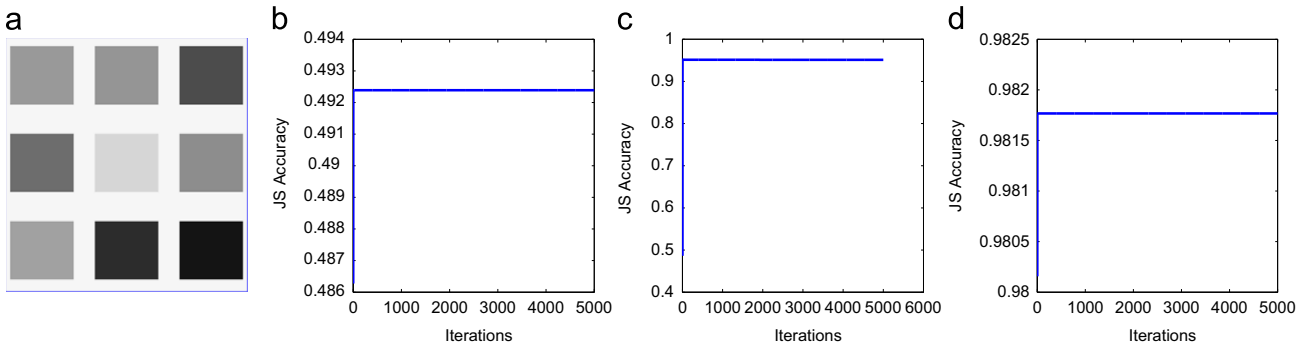

Fig. 20. Comparison 10 of three models in segmenting a synthetic multiphase type image: (a) Original image of size 256 × 256; (b) result of the FGM method (JS=0.492); (c) result of the LCV method (JS=0.95); (d) result of the DMD method (JS=0.98).

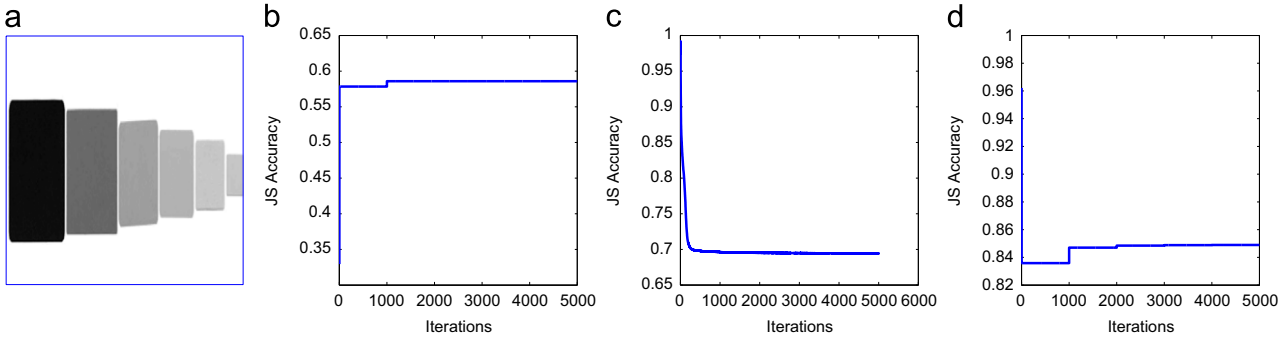

Fig. 21. Comparison 11 of three models in segmenting a synthetic multiphase type image: (a) Original image of size 256 × 256; (b) result of the FGM method (JS=0.6); (c) result of the LCV method (JS=0.7); (d) result of the DMD method (JS=0.85).

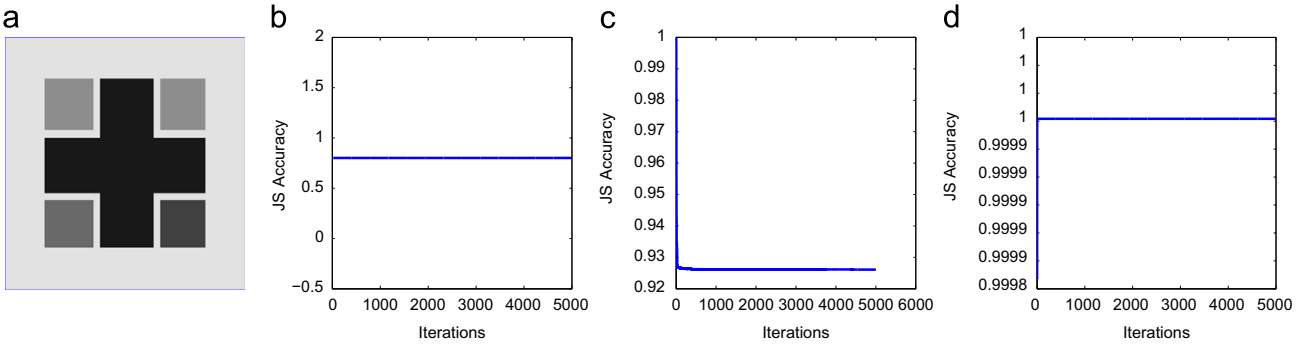

Fig. 22. Comparison 12 of three models in segmenting a synthetic multiphase type image: (a) Original image of size 256 × 256; (b) result of the FGM method (JS=0.7); (c) result of the LCV method (JS=0.6); (d) result of the DMD method (JS=0.72).

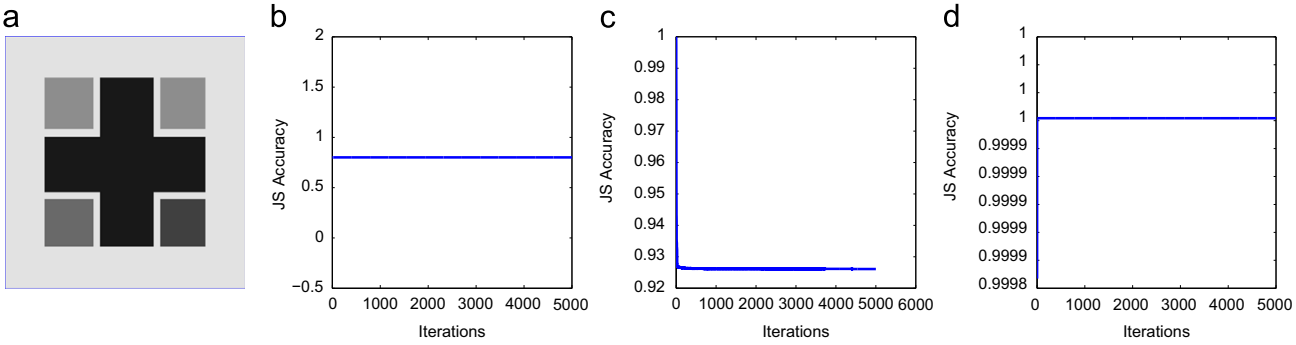

Fig. 23. Comparison 13 of three models in segmenting a real hardware image: (a) Original image of size 256 × 256; (b) result of the FGM method (JS=0.974); (c) result of the LCV method (JS=0.856); (d) result of the DMD method (JS=0.999).

multi-phase type images. Denote the segmented result, the set of pixels in object $\Omega_1 = inside(\Omega)$, by R_1 obtained by a model and the ground truth by R_2. The JS between the two regions R_1 and R_2 is termed as the ratio of the areas of the intersection by the union of the regions, i.e., $JS(R_1, R_2) = \frac{|R_1 \cap R_2|}{|R_1 \cup R_2|}$. To quantitatively evaluate the segmentation performance, we compute this JS quantity.

The closer the value of the JS to 1, the better the quality of the segmentation is. The JS tests can be seen in Figs. 18–23 where all the three models are tested on simple two and multi-phase images. For instance, the horizontal line in Fig. 18(b) shows the iterations and vertical line describes the JS values. These test results validate quantitatively the outstanding performance of the DMD model in comparison with the competing models.

7. Conclusions

We have proposed a new variational DMD model suitable for segmenting a range of images that have intensity inhomogeneity and multi-phases within objects. Previous works that can tackle problems with certain degree of intensity inhomogeneity include the LCV model [20] and the FGM model [3]. For ideal images with piecewise constant intensities, all three models give equally successful results. Beyond these images, comparisons have shown that our new DMD model is the only one that can deliver the expected segmentation quality and it behaves like the MS model for segmenting noisy images with piecewise smooth intensities, though it resembles the two-phase CV model. Equipped with global formulation this model is independent of initial contours and can tackle low contrast, noisy, inhomogeneous two-phase and many multi-phase type images.

Conflict of interest

None declared.

References

[1] N. Badshah, K. Chen, H. Ali, G. Murtaza, Coefficient of variation based image selective segmentation using active contour, East Asian J. Appl. Math. 2 (2) (2012) 150–169.
[2] T.F. Chan, L.A. Vese, Active contours without edges, IEEE Trans. Image Process. 10 (2) (2001) 266–277.
[3] X. Bresson, S. Esedoglu, P. Vandergheynst, J.-P. Thiran, S. Osher, Fast global minimization of the active contour/snake model, J. Math. Imaging Vis. 28 (2) (2007) 151–167.
[4] M. Jeon, M. Alexander, W. Pedrycz, N. Pizzi, Unsupervised hierarchical image segmentation with level set and additive operator splitting, Pattern Recognit. Lett. 26 (10) (2005) 1461–1469.
[5] D. Mumford, J. Shah, Optimal approximation by piecewise smooth functions and associated variational problems, Commun. Pure Appl. Math. 42 (1989) 577–685.
[6] G. Murtaza, H. Ali, N. Badshah., A robust local model for segmentation based on coefficient of variation, J. Inf. Commun. Technol. 5 (1) (2011) 30–39.
[7] B. Wu, X. Ji, D. Zhang, Fast two-phase image segmentation based on diffusion equations and gray level sets, Bound. Value Probl. 11 (2014) 1–16.
[8] M. Kass, A. Witkin, D. Terzopoulos, Active contours models, Int. J. Comput. Vis. 1 (4) (1988) 321–331.
[9] R. Adams, L. Bischof, Seeded region growing, IEEE Trans. Pattern Anal. Mach. Intell. 16 (6) (1994) 641–647.
[10] L. Vincent, L. Soille, Watersheds in digital spaces—an efficient algorithm based on immersion, IEEE Trans. Pattern Anal. Mach. Learn. 6 (1994) 583–598.
[11] E. Zagrouba, S.B. Gamra, A. Najjar, Model-based graph-cut method for automatic flower segmentation with spatial constraints, Image Vis. Comput. 32 (12) (2014) 1007–1020.
[12] O. Eches, J.A. Benediktsson, N. Dobigeon, J.Y. Tourneret, Adaptive Markov random fields for joint unmixing and segmentation of hyperspectral images, IEEE Trans. Image Process. 22 (1) (2013) 5–16.
[13] K. Zhang, H. Song, L. Zhang, Active contours driven by local image fitting energy, Pattern Recognit. 43 (4) (2010) 1199–1206.

[14] C. Gout, C.L. Guyader, L.A. Vese, Segmentation under geometrical conditions with geodesic active contour and interpolation using level set method, Numer. Algorithms 39 (2005) 155–173.
[15] C.L. Guyader, C. Gout, Geodesic active contour under geometrical conditions theory and 3D applications, Numer. Algorithms 48 (2008) 105–133.
[16] V. Caselles, R. Kimmel, G. Sapiro, Geodesic active contours, Int. J. Comput. Vis. 22 (1) (1997) 61–79.
[17] C. Li, C. Xu, C. Gui, M.D. Fox, Level set evolution without re-initialization: a new variational formulation, in: IEEE Computer Society Conference on Computer Vision and Pattern Recognition, vol. 1, 2005, pp. 430–436.
[18] S. Osher, J.A. Sethian, Fronts propagating with curvature-dependent speed: algorithms based on HJ formulations, J. Comput. Phys. 79 (1) (1988) 12–49.
[19] J.A. Sethian, Level set methods and fast marching methods, in: Evolving Interfaces in Computational Geometry, Fluid Mechanics, Computer Vision and Material Science, Cambridge University Press, New York, 1999.
[20] X.F. Wang, D.S. Huang, H. Xu, An efficient local Chan-Vese model for image segmentation, Pattern Recognit. 43 (2010) 603–618.
[21] T. Lu, P. Neittaanmaki, X.C. Tai, A parallel splitting up method and its application to Navier–Stokes equations, Appl. Math. Lett. 4 (2) (1991) 25–29.
[22] J. Weickert, B.M. ter Haar Romeny, M.A. Viergever, Efficient and reliable schemes for nonlinear diffusion filtering, IEEE Trans. Image Process. 7 (1998) 398–410.
[23] J. Weickert, G. Kuhne, Fast methods for implicit active contours models, in: Geometric Level Set Methods in Imaging, Vision, and Graphics, 2003, pp. 43-58.
[24] K. Chen, Matrix Preconditioning Techniques and Applications, Cambridge University Press, New York, 2005.
[25] A. Chambolle, D. Cremers, T. Pock, A convex approach to minimal partitions, SIAM J. Imaging Sci. 5 (4) (2012) 1113–1158.
[26] Y. Gu, L.L. Wang, X.C. Tai, A direct approach towards global minimization for multiphase labeling and segmentation problems, IEEE Trans. Image Process. 21 (5) (2012) 2399–2411.
[27] L.A. Vese, T.F. Chan., A multiphase level set framework for image segmentation using the Mumford and Shah model, Int. J. Comput. Vis. 50 (3) (2002) 271–293.

Haider Ali is a Ph.D. Student in the Department of Mathematics, University of Peshawar, Pakistan.

Noor Badshah is an Assistant Professor in the Department of Basic Sciences, UET Peshawar, Pakistan.

Ke Chen is a Professor in the Department of Mathematical Sciences, University of Liverpool, United Kingdom.

Gulzar Ali Khan is a Professor in the Department of Mathematics, University of Peshawar.